Int. Symposium on Gas–Particle Flows,
ASME Fluids Engineering Division Summer Meeting, FEDSM'97
June 22-26, 1997, Vancouver (BC), Canada
CD–ROM Proceedings, FEDSM97–3590

A 3–DIMENSIONAL LAGRANGIAN SOLVER FOR DISPERSE MULTIPHASE FLOWS ON ARBITRARY, GEOMETRICALLY COMPLEX FLOW DOMAINS USING BLOCK–STRUCTURED NUMERICAL GRIDS

Th. Frank, E. Wassen, Q. Yu
Faculty of Mechanical Engineering and Process Technology
Research Group of Multiphase Flow
Technical University of Chemnitz–Zwickau
Chemnitz, Germany
Phone: +49 371 531 4643
Fax: +49 371 531 4644
E-Mail: frank@imech.tu-chemnitz.de

ABSTRACT

A Lagrangian solver for the numerical simulation of disperse multiphase flows is presented. The solver is applicable to the prediction of flows in complex geometries. The flow domain is descretized by a block-structured numerical grid consisting of arbitrary hexahedral control volumes. Emphasis is layed on the treatment of geometrical issues. In a boundary fitted grid the corner points of the control volume faces do not necessarily form a flat surface. For porpuses of particle localization and particle tracing the representation of the control volume is changed to a dodecahedral one. Two different methods are presented for the localization of a particle's initial position in a grid block. Further an efficient algorithm is given for tracing a particle on the numerical grid. By using this algorithm the source terms due to particle-fluid interaction can be calculated simultanously when searching the new particle location. Test case calculations are presented for the flow in a cyclone seperator.

NOMENCLATURE

C_D, C_A, C_M	coefficients
H_r	roughness height
L_r	roughness lenght
Re	Reynolds number
S_Φ	source term
S_Φ^P	source term due to particle-fluid interaction
V	volume
e	koefficient of restitution
f	koefficient of kinetic friction
g	gravitational acceleration
k	turbulence kinetic energy
m	mass
t	time
u, v, w	velocity in x-, y- and z-direction
v_{rel}	absolute value of particle-fluid relative velocity
Γ	generall transport coefficient
Φ	general variable in transport equation
Ω	fluid rotation
γ	inclination angle of rough wall
ϵ	dissipation
ν	kinematic viscosity
ξ_m	coefficient
ρ	density
ω	particle rotational velocity
ω_{rel}	absolute value of particle-fluid relative rotational velocity

Subscripts

F	fluid
P	particle

1. INTRODUCTION

There are many flow situations in mechanical engineering and process technology where disperse multiphase flows play an important role. In many cases particulate two–phase flows have to be predicted in large scale facilities with geometrically complex flow domains. Real flow regimes are 3–dimensional and cannot be restricted to 2–dimensional numerical studies. Examples for such complex flow regimes can be found e.g. in particle separators/cyclones or in pulverized coal fired furnaces.

The objective of this work was to develop an Eulerian/Lagrangian approach for the numerical prediction of 3–dimensional, particulate two–phase flows. Special attention was payed to aspects of geometrical representation and approximation of the flow domain, to algorithms for particle localization on a 3–dimensional numerical grid, for particle tracking throughout a complex geometry and for the particle–wall interaction with an arbitrary inclined wall in 3–dimensional space. All developments were carried out having in mind that the parallelization methods developed in [Frank, 1996, Frank and Wassen, 1996] for 2–dimensional, disperse multiphase flow simulations should be applicable to the 3–dimensional algorithm as well.

2. SOLUTION OF THE EQUATIONS OF FLUID MOTION

The two–phase (gas–particle) flow under consideration is described by assuming that the particulate phase is dilute, but the particle loading can be appreciable. Inter–particle effects are neglected, but the effect of the particles on the gas flow are taken into account by the PSI–Cell approach [Crowe et al., 1977, Crowe, 1982]. The two–phase flow is statistically steady, incompressible and isothermal. Under these assumptions the time–averaged form of the governing gas–phase equations can be expressed in the form of the general transport equation :

$$\frac{\partial}{\partial x}(\rho_F\, u_F\, \Phi) + \frac{\partial}{\partial y}(\rho_F\, v_F \Phi) + \frac{\partial}{\partial z}(\rho_F\, w_F \Phi) = \frac{\partial}{\partial x}\left(\Gamma \frac{\partial \Phi}{\partial x}\right) + \frac{\partial}{\partial y}\left(\Gamma \frac{\partial \Phi}{\partial y}\right) + \frac{\partial}{\partial z}\left(\Gamma \frac{\partial \Phi}{\partial z}\right) + S_\Phi + S_\Phi^P \qquad (1)$$

where Φ stands for u_F, v_F, w_F, k and ε. The terms S_Φ and Γ are discussed in more detail in [Frank and Wassen, 1996]. S_Φ^P represents the coupling of both phases and is calculated by solving the Lagrangian equations of particle motion using the PSI–cell–method [Crowe et al., 1977, Frank and Wassen, 1996].

The above equations of fluid motion are solved by the program package FAN–3D developed by Perić and Lilek [Perić and Lilek, 1993]. FAN–3D is basically the 3–dimensional extension of the 2–dimensional algorithm described in [Perć, 1989, Perić, 1992]. The most fundamental features of FAN–3D are :

- use of non–orthogonal, boundary fitted, numerical grids with arbitrary hexahedral control volumes (see Fig. 1),
- use of block structured numerical grids for optimum geometrical approximation of complex flow domains and for parallelization purposes;
- colocated variable arrangement; Cartesian vector and tensor components;
- finite volume solution approach of SIMPLE kind [Perić, 1992, Patankar, 1980].

3. THE 3–DIMENSIONAL LAGRANGIAN APPROACH

3.1. Equations of motion of the dispersed phase

The disperse phase is treated by the Lagrangian approach where a large number of particles is calculated throughout the flow domain. Each particle trajectory represents a fraction of the overall particle mass loading expressed by the particle number flow rate $\dot{N}_P$ along the calculated trajectory. For the formulation of particles equations of motion a small density ratio ρ_F/ρ_P is assumed. So the drag force, the lift force due to particle rotation (Magnus force), the lift force due to shear in the fluid flow (Saffman force), the gravitational and added mass force are taken into account [Frank, 1992, Tsuji et al., 1991].

$$\frac{d}{dt}\begin{bmatrix} x_P \\ y_P \\ z_P \end{bmatrix} = \begin{bmatrix} u_P \\ v_P \\ w_P \end{bmatrix} \qquad (2)$$

$$\frac{d}{dt}\begin{bmatrix} u_P \\ v_P \\ w_P \end{bmatrix} = \frac{3}{4}\frac{\rho_F}{(\rho_P + \rho_F/2) d_P}\left(v_{rel} C_D(Re_P) \begin{bmatrix} u_F - u_P \\ v_F - v_P \\ w_F - w_P \end{bmatrix} + \frac{v_{rel}}{\omega_{rel}} C_M(\sigma) \cdot \right.$$

$$\left[\begin{array}{c} (v_F - v_P)(\omega_z - \Omega_z) - (w_F - w_P)(\omega_y - \Omega_y) \\ (w_F - w_P)(\omega_x - \Omega_x) - (u_F - u_P)(\omega_z - \Omega_z) \\ (u_F - u_P)(\omega_y - \Omega_y) - (v_F - v_P)(\omega_x - \Omega_x) \end{array} \right]$$

$$+ \quad \frac{2\nu^{1/2}}{\pi\Omega^{1/2}} C_A \left[\begin{array}{c} (v_F - v_P)\Omega_z - (w_F - w_P)\Omega_y \\ (w_F - w_P)\Omega_x - (u_F - u_P)\Omega_z \\ (u_F - u_P)\Omega_y - (v_F - v_P)\Omega_x \end{array} \right] \Bigg)$$

$$+ \quad \frac{\rho_P - \rho_F}{\rho_P + \rho_F/2} \left[\begin{array}{c} g_x \\ g_y \\ g_z \end{array} \right] \qquad (3)$$

$$\frac{d}{dt} \left[\begin{array}{c} \omega_x \\ \omega_y \\ \omega_z \end{array} \right] = -\frac{15}{16\pi} \frac{\rho_F}{\rho_P} \omega_{rel} \xi_m \left[\begin{array}{c} \omega_x - \Omega_x \\ \omega_y - \Omega_y \\ \omega_z - \Omega_z \end{array} \right] \qquad (4)$$

with :

$$Re_P = \frac{d_P\, v_{rel}}{\nu} \quad , \quad v_{rel} = \sqrt{(u_F - u_P)^2 + (v_F - v_P)^2} \quad ,$$

$$\sigma = \frac{1}{2} \frac{d_P \omega}{v_{rel}} \qquad , \qquad \xi_m = \xi_m(Re_\omega) \quad ,$$

$$\omega_{rel} = \sqrt{(\omega_x - \Omega_x)^2 + (\omega_y - \Omega_y)^2 + (\omega_z - \Omega_z)^2}$$

The various coefficients C_D, C_M, C_A, ξ_m in the above equations and other model constants, e.g. restitution coefficient e and coefficient of kinetic friction f in the particle–wall collision model are taken from literature [Frank, 1992]. The effect of turbulence of the fluid flow on the motion of the dispersed phase is simulated by the Lagrangian stochastic–deterministic (LSD) turbulence model [Milojević, 1990].The general numerical solution procedure for the coupled system of fluid and particles equation of motion is described in detail in [Frank and Wassen, 1996] and is applicable to the 3-dimensional flow simulation as well.

But for a successful adaptation of this numerical approach to the 3–dimensional representation of the flow domain geometry some basic problems have to be solved :

- efficient particle localization algorithms to find particle initial conditions on the numerical grid;
- particle tracing algorithm for particle trajectory calculation throughout the flow domain, which is divided in several grid blocks;
- efficient interpolation of fluid flow properties at the current particle location;
- treatment of particle–wall collisions with arbitrary inclined wall surfaces;
- calculation of source terms for particle–fluid interaction and of mean properties of the dispersed phase for data analysis and post–processing purposes.

3.2. Control volumes and the numerical grid

The numerical approach of FAN–3D is based on a finite volume discretization scheme for the general transport equation (1). Therefore the block–structured numerical grid consists of hexahedral control volumes (CV) which can be regarded as topological equivalent to cubes (see Fig. 1). The grid blocks can be arbitrarily interconnected with the only limitation, that a face of a CV on one side of such an inter–block boundary has a corresponding cell face on the neighbouring grid block boundary. In general the quadrangular faces of the single CV's are not plane surfaces. But the only information given about the shape of this cell faces by the numerical grid representation are the coordinates of the 4 corner points.

For the particle trajectory calculations this representation of a CV is complemented by 6 diagonals of the faces (Fig. 1) converting every CV to a dodecahedron with plane triangular faces. This leads to a well–determined subdivision of the flow domain in finite volumes without overlapping regions and "empty space" between CV's. Now this subdivision allows a well–defined assignment between a certain particle location in space and the corresponding CV on the numerical grid. Furthermore the conversion of hexahedral to dodecahedral CV's allows the decomposition of a CV in 6 tetrahedral sub–CV's (Fig. 2). This decomposition can be used for efficient implementation of geometrical algorithms for the 'point-inside-a-polyhedron' problem.

3.3. Localization of the particle initial conditions

In order to start the Lagrangian particle trajectory calculation it is neccessary to find the corresponding CV on the numerical grid for each particle initial condition $P_I = (x_{PI}, y_{PI}, z_{PI})$ with the particle state $(\vec{v}_{PI}, \vec{\omega}_{PI}, d_{PI}, \dot{N}_{PI}, T_{PI}, \ldots)$. For orthogonal numerical grids with cell faces parallel to the coordinate axes the problem can easily be solved by comparing the grid line coordinates of a certain grid block with the coordinates of the initial condition P_I :

$$x_{i-1} \le x_{PI} \le x_i, \quad y_{j-1} \le y_{PI} \le y_j, \quad z_{k-1} \le z_{PI} \le z_k$$

For complex 3–dimensional grids of the given type the problem is much more complicated. There are two basic methods for the point–location problem.

Method a) :

This method was proposed by Preparata et al. in

[Preparata and Shamos] and is called the 'single–shot approach'. Consider that it has to be determined wether the particle initial condition P_I lies inside a certain part of the numerical grid or not. Therefor we pass a ray from P_I to a point P_∞ outside of the whole grid geometry (Fig. 3). Now all crosspoints S_i of ray $\overrightarrow{P_I P_\infty}$ with the surface of the grid substructure can be determined. As mentioned above this surface consists of the triangular faces of the included dodecahedral CV's. It can be shown that P_I lies inside this grid substructure if the number of intersections S_i is odd. Starting the analysis with a single grid block of the numerical grid a progressive bisection leads to the CV which corresponds to the coordinates of P_I (Fig. 4).

If N^3 is the number of CV's in a grid block than it is straightforward to recognize that the numerical effort for this method $E_N \sim O(N^2)$ for an almost cubic arrangement of grid cells. But E_N can increase to $O(N^3)$ for the worst case when grid cells are arranged in a single row. Further it has to be mentioned that the method is 'fragil' in some sense. If the ray $\overrightarrow{P_I P_\infty}$ passes through an edge or corner or is parallel to a face of the grid substructure under investigation the method gives no result. This problem can only be solved by changing the coordinates of the point P_∞.

Method b) :

This approach is based upon the fact, that the position of a point to a plane surface can easily be determined from its normal equation. Applying this to the four faces of a tetrahedron and subsequently to the six tetrahedral sub–CV's of a dodecahedral CV it can be decided wether a point P_I lies inside a certain CV of our numerical grid or not. This method is 'robust', that means it can be applied under all circumstances to any combination of particle initial conditions P_I and control volumes of the numerical grid. But unfortunately the numerical effort of this method is always $E_N \sim O(N^3)$.

A comparison of both methods shows that method a) is very efficient for larger grid substructures with a total number of grid cells greater than 10^2. If the progressive bisection of method a) leeds to smaller grid substructures method b) is more advantageous.

3.4. Particle tracing and calculation of source terms

If the particle initial conditions are localized on the numerical grid the particle equations of motion (2)–(4) can be solved using a standard Runge–Kutta solution scheme of 4th order accuracy with automatic time step correction.

For a given particle location $P_1(t)$ the new calculated particle location $P_2(t+\Delta t)$ has to be assigned to its corresponding CV on the numerical grid. First for the CV corresponding to $P_1(t)$ all intersections of $\overrightarrow{P_1 P_2}$ with the CV faces for which the scalar product $(\vec{n}, \overrightarrow{P_1 P_2}) \geq 0$ have to be determined, where $\vec{n}$ is the outer normal vector of the CV face. The particle trajectory leaves the CV surrounding $P_1(t)$ through the face for which $|\overrightarrow{P_1 S_i}|$ is minimal. This leeds to the next neighbouring CV crossed by the particle path $\overrightarrow{P_1 P_2}$. Applying this method subsequently to all neighbouring CV's which are crossed by the particle path $\overrightarrow{P_1 P_2}$ leeds to the CV surrounding the new particle location $P_2(t+\Delta t)$. Fortunately this particle tracing procedure can simultanously be used for the calculation of the source terms due to particle–fluid interaction, since as a result of the particle tracing procedure all intersections of the particle trajectory segment $\overrightarrow{P_1 P_2}$ with CV faces lying between these two particle states are determined. This allows simultanous summation of source term contributions :

$$S_{u_i}^P = -\frac{1}{V_{ij}} \sum m_P \dot{N}_P \cdot \left[u_{Pi,out} - u_{Pi,in} - g_i \frac{\rho_P - \rho_F}{\rho_P + \rho_F/2} (t_{out} - t_{in}) \right] \quad (5)$$

for the grid cells crossed by the particle trajectory segment $\overrightarrow{P_1 P_2}$ during the Runge–Kutta time step Δt. The particle properties at the intersections S_i have to be linearly interpolated along $\overrightarrow{P_1 P_2}$. The value of the fluid flow variable Φ at a certain particle location $P = (x_P, y_P, z_P)$ has to be interpolated from the value of Φ in the corresponding CV by :

$$\begin{aligned} \Phi|_P &= \Phi|_{CV} + \left.\frac{\partial \Phi}{\partial x}\right|_{CV} (x_P - x_C) \\ &+ \left.\frac{\partial \Phi}{\partial y}\right|_{CV} (y_P - y_C) + \left.\frac{\partial \Phi}{\partial z}\right|_{CV} (z_P - z_C) \end{aligned} \quad (6)$$

where $\vec{r}_C = (x_C, y_C, z_C)$ are the coordinates of the CV centre point.

3.5. Particle–wall interaction

The majority of industrially important disperse multiphase-flows are confined flows, e.g. flows in cyclone seperators or in pneumatic conveying pipe systems. Especially the motion of large particles, which is dominated by inertia, is strongly influenced by the confinement. Considering the wall-collision process it has been shown that irregularities due to wall-roughness and/or deviation of particle shape from sphere play an important role [Frank, 1992, Matsumoto et al., 1976, Tsuji et al., 1985].

In this study the particle-wall collisions are simulated according to the irregular bouncing model by Sommerfeld

[Sommerfeld, 1992]. The particle collides with an inclined virtual wall. The inclination angle γ is sampled from a Gaussian distribution with a mean value of 0° and a standard deviation of $\Delta\gamma$. $\Delta\gamma$ depends on the particle diameter d_P and the roughness parameters and may be estimated by:

$$\begin{aligned} \Delta\gamma = &\quad \arctan\tfrac{2\Delta H_r}{L_r} \qquad \text{for} \quad d_P \geq \frac{L_r}{\sin(\arctan\frac{2H_r}{L_r})} \\ \Delta\gamma = &\quad \arctan\tfrac{2H_r}{L_r} \qquad \text{for} \quad d_P < \frac{L_r}{\sin(\arctan\frac{2H_r}{L_r})} \end{aligned} \tag{7}$$

Here L_r is the mean cycle of roughness, H_r is the mean roughness height and ΔH_r is the standard deviation of the roughness height. Since no preferential direction of roughness is assumed, the inclined virtual wall is additionally turned around the normal vector of the original wall by an azimuthal angle σ_a. This azimuthal angle is sampled from a uniform distribution in the range $[-\pi, \pi]$.

The particle velocities and angular velocities are transformed to a coordinate system that is aligned with the collision plane. For the following equations it is assumed that the y-axis of the transformed coordinate system is identical to the normal vector of the collision plane. The computation of the velocities and angular velocities after rebound is carried out by applying the impulse equations and taking into account the sort of collision, i.e. sliding or non-sliding collision [Tsuji et al., 1985]:

1. sliding collision for : $-\frac{2}{7\,f\,(e+1)} \leq \frac{v_p^{(1)}}{|v_r|} \leq 0$:

$$\begin{aligned} u_p^{(2)} &= u_p^{(1)} + \epsilon_x\, f\,(e+1)\, v_p^{(1)} \quad , \\ v_p^{(2)} &= -\,e\, v_p^{(1)} \quad , \\ w_p^{(2)} &= w_p^{(1)} + \epsilon_z\, f\,(e+1)\, v_p^{(1)} \quad , \\ \omega_x^{(2)} &= \omega_x^{(1)} - \frac{5}{d_p}\,\epsilon_z\, f\,(e+1)\, v_p^{(1)} \quad , \\ \omega_y^{(2)} &= \omega_y^{(1)} \quad , \\ \omega_z^{(2)} &= \omega_z^{(1)} + \frac{5}{d_p}\,\epsilon_x\, f\,(e+1)\, v_p^{(1)} \end{aligned} \tag{8}$$

2. non-sliding collision for : $\frac{v_p^{(1)}}{|v_r|} < -\frac{2}{7\,f\,(e+1)}$:

$$\begin{aligned} u_p^{(2)} &= \frac{5}{7}\,(u_p^{(1)} - \frac{d_p}{5}\,\omega_z^{(1)}) \quad , \\ v_p^{(2)} &= -\,e\, v_p^{(1)} \quad , \\ w_p^{(2)} &= \frac{5}{7}\,(w_p^{(1)} + \frac{d_p}{5}\,\omega_x^{(1)}) \quad , \\ \omega_x^{(2)} &= \frac{2}{d_p}\, w_p^{(1)} \quad , \\ \omega_y^{(2)} &= \omega_y^{(1)} \quad , \\ \omega_z^{(2)} &= -\,\frac{2}{d_p}\, u_p^{(1)} \end{aligned} \tag{9}$$

with :

$$|v_r| = \sqrt{(u_p^{(1)} + \frac{d_p}{2}\,\omega_z^{(1)})^2 + (w_p^{(1)} - \frac{d_p}{2}\,\omega_x^{(1)})^2}$$

and :

$$\epsilon_x = \frac{u_p^{(1)} + \frac{d_p}{2}\,\omega_z^{(1)}}{|v_r|} \quad , \quad \epsilon_z = \frac{w_p^{(1)} - \frac{d_p}{2}\,\omega_x^{(1)}}{|v_r|}$$

In these equations e is the coefficient of restitution and f is the coefficient of kinetic friction. The superscripts (1) and (2) indicate values before and after collision, respectively.

4. PARALLELIZATION

In [Frank, 1996, Frank and Wassen, 1996] was shown that the Eulerian/Lagrangian approach for numerical simulations of disperse multiphase flows is well suited for calculations on massively parallel computers (MIMD). This is even more important in the case of complex 3–dimensional flow situations. Both parallelization methods investigated in [Frank and Wassen, 1996] are applicable to the 3–dimensional Lagrangian approach presented in this paper without limitations. Because parallelization of the Lagrangian approach is carried out by parallelization in space using the domain decomposition method the described algorithms are applicable to steady and unsteady flow calculations as well.

5. GAS–PARTICLE FLOW IN A STANDARD CYCLONE

The 3-dimensional Lagrangian approach was applied to the gas–particle flow in a standard cyclon (Fig. 6). The test case calculations were based on experimental investigations of precipitation rates of a series of geometrically similiar cyclons published in literature [König, 1990]. The geometry of the cyclon investigated in this paper was determined by:

Diameter of the cyclon	$D = 40\ mm$
Height of the cyclon	$H = 195\ mm$
Inlet cross section	$a \times b = 4.5\ mm \times 18\ mm$
Diameter of the gas exit	$d_T = 10\ mm$
Height of the gas exit	$h_T = 31\ mm$
Diameter of the particle exit	$d_B = 10\ mm$

Calculations were performed for different inlet gas velocities of $\overrightarrow{v_F}$= 5 m/s to $\overrightarrow{v_F}$= 25 m/s with the corresponding

volume flow rates of 1.46 m^3/h to 7.29 m^3/h. For the disperse phase a fraction of quartz particles was used with the given particle diameter distribution from [König, 1990] and a mean particle diameter of $d_P = 10.9\ \mu m$.

Due to the complex geometry of the cyclon a numerical grid with 42 different grid blocks was designed for the numerical calculations of the gas-particle flow (Fig. 7). The first calculations agree qualitatively well with experiments (Fig. 8).

6. CONCLUSIONS

The paper gives the formulation of a 3–dimensional Lagrangian approach applicable to flow domains with complex geometrical boundary conditions. The treatment of particle localization, particle tracing and particle–wall interaction on 3–dimensional, block–structured, boundary fitted numerical grids are discussed in detail.

The Lagrangian approach is applied to the gas–particle flow in a standard cyclone. Results for particle precipitation rates show the applicability of the approach to complex 3–dimensional multiphase flows.

7. ACKNOLEDGEMENT

The authors are indebted to Prof. M. Perić for allowing the use of his CFD code FAN–3D in this research. Further this work was supported by the Deutsche Forschungsgemeinschaft (DFG) under Contract No. SFB 393/D2 and No. Fr 1069/3–1.

REFERENCES

[Crowe et al., 1977] Crowe C.T., Sharma M.P., Stock D.E., 1977, "The Particle–Source–In Cell (PSI–Cell) Model for Gas–Droplet Flows," *Trans. of ASME, J. Fluids Eng.,* Vol. 99, pp. 325–332.

[Crowe, 1982] Crowe C.T., 1982, "REVIEW — Numerical Models for dilute Gas–Particle Flows," *Trans. of ASME, J. Fluids Eng.,* Vol. 104, pp. 297–303.

[Frank, 1992] Frank Th, 1992 "Numerische Simulation der feststoffbeladenen Gasströmung im horizontalen Kanal unter Berücksichtigung von Wandrauhigkeiten", PhD Thesis, Techn. University Bergakademie Freiberg, Germany.

[Frank, 1996] Frank Th., 1996, "Comparison of three parallelization methods for calculation of disperse multiphase flows using the Lagrangian approach", *Proc. 3rd Int. Conference "Parallel CFD '96"*, Implementations and Results Using Parallel Computers, Capri, Italy, May 20–23, 1996.

[Frank and Wassen, 1996] Frank Th., Wassen E., 1996, "Parallel Solution Algorithms for Lagrangian Simulation of Disperse Multiphase Flows", *Proc. 2nd Int. Symposium on Numerical Methods for Multiphase Flows*, ASME Fluids Engineering Division Summer Meeting, San Diego, CA, USA, July 7–11, 1996, Vol. 1, pp. 11–20.

[König, 1990] König, 1990, "Untersuchungen zum Abscheideverhalten von geometrisch ähnlichen Zyklonen", PhD at the University of Kaiserslautern, Germany.

[Matsumoto et al., 1976] Matsumoto S., Saito S., Maeda S., 1976, "Simulation of gas–solid two–phase flow in horizontal pipe", *Journal of Chemical Engineering of Japan*, Vol. 9, No. 1, pp. 23–28.

[Milojević, 1990] Milojević D., 1990, "Lagrangian Stochastic–Deterministic (LSD) Predictions of Particle Dispersion in Turbulence," *Part. Part. Syst. Charact.,* Vol. 7, pp. 181–190.

[Patankar, 1980] Patankar S.V., 1980, "Numerical Heat Transfer and Fluid Flow", McGraw–Hill, New York.

[Perć, 1989] Perić M., 1989, "A Finite Volume Multigrid Method for Calculating Turbulent Flows," *Proc. 7th Symposium on Turbulent Shear Flows,* Vol. 1, pp. 7.3.1.–7.3.6., Stanford University, USA.

[Perić, 1992] Perić M., 1992, "Ein zum Parallelrechnen geeignetes Finite–Volumen–Mehrgitterverfahren zur Berechnung komplexer Strömungen auf blockstrukturierten Gittern mit lokaler Verfeinerung", Abschlußbericht zum DFG–Vorhaben Pe 350/3–1 im DFG–Habilitandenstipendiumprogramm, Stanford University, USA.

[Perić and Lilek, 1993] Perić M., Lilek Ž., 1993, "Users Manual for the FAN–2D Software for the Calculation of Incompressible Flows", Institut für Schiffbau der Universität Hamburg, Germany.

[Preparata and Shamos] Preparata F.P., Shamos M.I. : "Computational Geometry – An Introduction", Texts and Monographs in Computer Science, Springer Verlag, New York.

[Sommerfeld, 1992] Sommerfeld M., 1992, "Modelling of particle–wall collisions in confined gas–particle flows", *Int. Journal of Multiphase Flows*, Vol. 18, No. 6, pp. 905–926.

[Tsuji et al., 1985] Tsuji Y., Oshima T., Morikawa Y., 1985, "Numerical simulation of pneumatic conveying in a horizontal pipe", *KONA – Powder Science and Technology in Japan*, No. 3, pp. 38–51.

[Tsuji et al., 1991] Tsuji Y., Shen N.Y., Morikawa Y., 1991, "Lagrangian Simulation of Dilute Gas–Solid Flows in a Horizontal Pipe", *Advanced Powder Technology*, Vol. 2, No. 1, pp. 63–81.

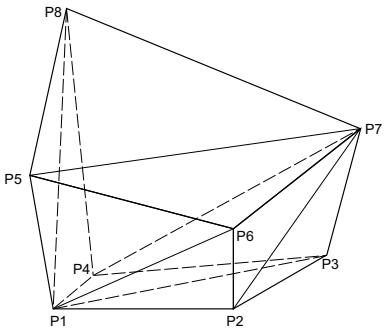

Figure 1: Shape of an arbitrary dodecahedral control volume of the numerical grid.

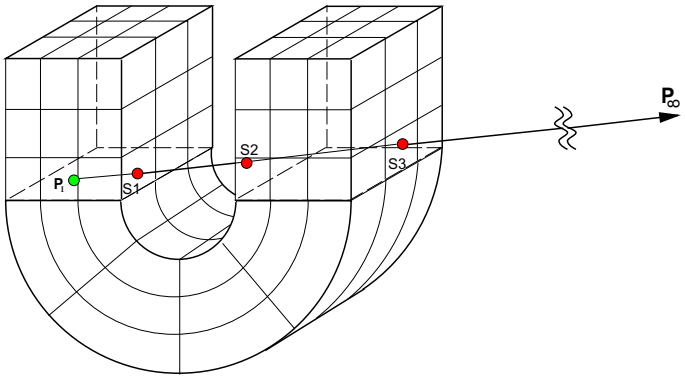

Figure 3: Localization of particle initial conditions on the numerical grid.

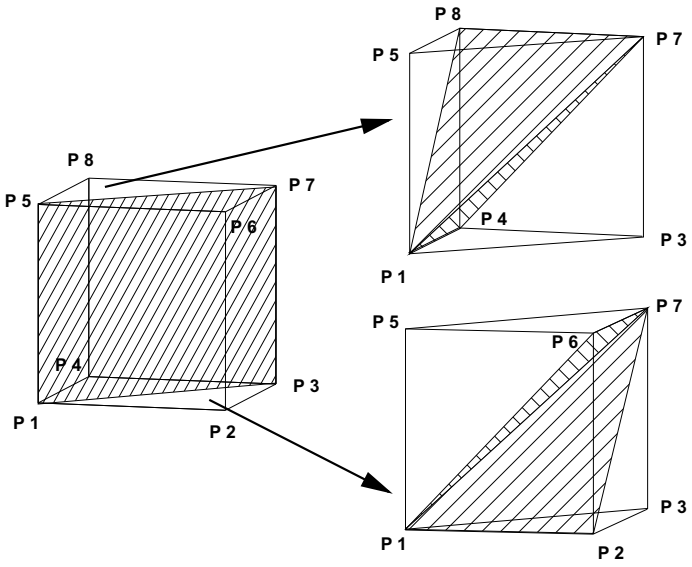

Figure 2: Decomposition of a dodecahedral control volume.

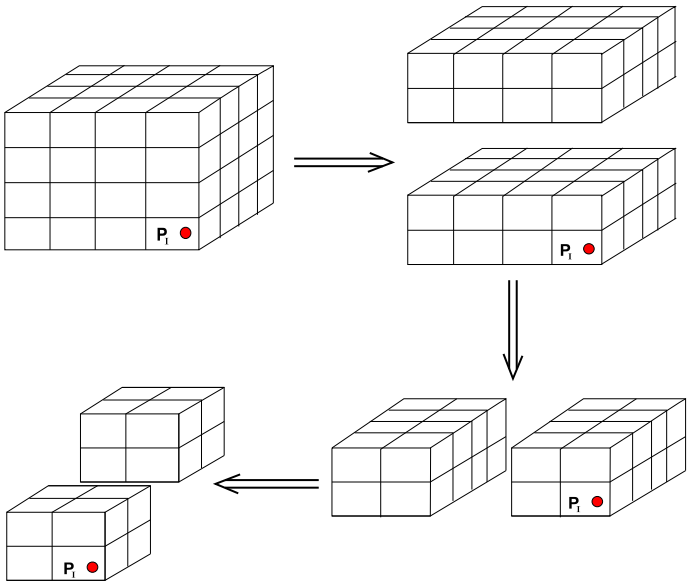

Figure 4: Search for particle position P_I by progressive bisection of the grid substructure.

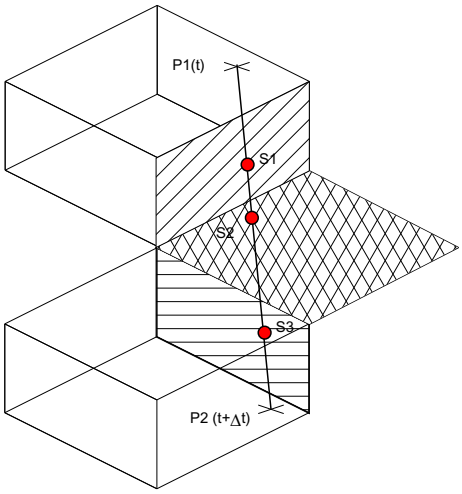

Figure 5: Particle tracing from a given location $P_1(t)$ to the new calculated particle location $P_2(t + \Delta t)$.

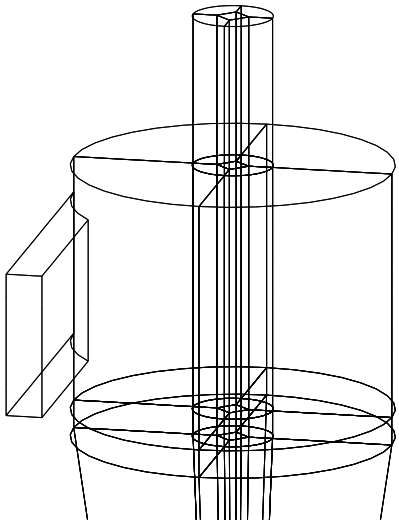

Figure 7: Block structure of the numerical grid in the upper part of the cyclon.

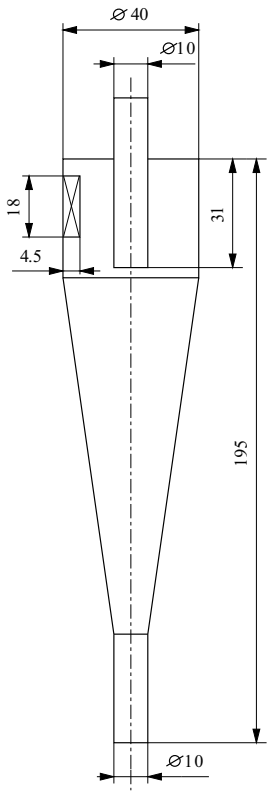

Figure 6: Scheme of the standard cyclon used in the gas-particle flow calculations for prediction of precipitation rate.

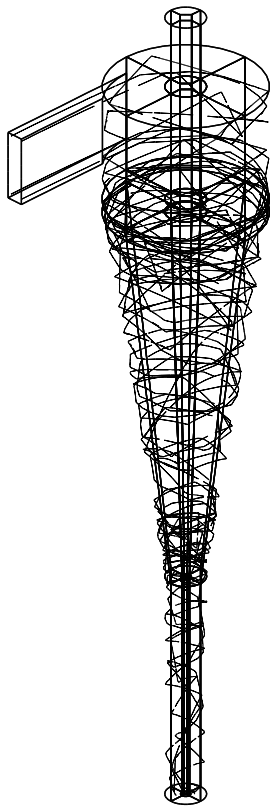

Figure 8: Calculated particle trajectories for inlet velocity 10 m/s.